Structure of a thin oxide film on Rh(100)

J. Gustafson,* A Mikkelsen, M. Borg, J. N. Andersen, and E. Lundgren
Department of Synchrotron Radiation Research, Lund University, Box 118, S-221 00, Sweden

C. Klein, W. Hofer, M. Schmid, and P. Varga
Institut für Allgemeine Physik, Technische Universität Wien, A-1040 Wien, Austria

L. Köhler and G. Kresse
Institut für Materialphysik, Universität Wien, A-1090 Wien, Austria

N. Kasper, A. Stierle, and H. Dosch
Max-Planck Institut für Metallforschung, Heisenbergstrasse 3, D-70569 Stuttgart, Germany
(Received 8 October 2004; published 31 March 2005)

The initial oxidation of Rh(100) has been studied using high resolution core level spectroscopy, low energy electron diffraction, surface x-ray diffraction, scanning tunneling microscopy, and density functional theory. We report a structural study of an oxygen induced structure displaying a $c(8\times2)$ periodicity at an oxygen pressure above 10^{-5} mbar and using a sample temperature of 700 K. Our experimental and theoretical data demonstrate that this structure is due to the formation of a thin surface oxide with a hexagonal trilayer O-Rh-O structure.

DOI: 10.1103/PhysRevB.71.115442 PACS number(s): 68.35.Bs, 79.60.−i, 68.37.Ef, 68.43.Bc

I. INTRODUCTION

Oxygen interactions with late transition metal surfaces under high oxygen partial pressures and elevated sample temperatures have recently received significant attention.[1–7] One major reason for this effort, apart from fundamental interest, has been the important role that oxygen plays in catalytic reactions, such as the CO conversion into CO_2, on metal surfaces. Recently, Ru, Pt, and Pd surfaces have been studied using higher partial oxygen pressures than traditionally used in surface science in order to approach conditions similar to those of a catalyst under working conditions. The studies have clearly demonstrated that the formation of oxides significantly increases the CO oxidation rate on these surfaces.[3–5] Obtaining an understanding of the formation, structure, and reactivity of late transition metal oxides is therefore of great interest.

The formation of thicker oxides on these surfaces has turned out to be more complicated than initially believed. In several cases, so-called surface oxides form[1,8–10] prior to the onset of thicker oxides. Some of these thin oxides display structures unrelated to the corresponding bulk oxides,[9] and in the case of Rh(111) as well as on Pd(001),[1,2] the presence of a surface oxide kinetically hinders the formation of the respective bulk oxide. Furthermore, the effect of these surface oxides on the catalytic reactivity of the metal surface is not clear at present.

A number of studies have been performed previously on the O/Rh(100) system.[11–16] The best documented superstructures are a $p(2\times2)$ at a coverage of $\theta=1/4$ ML [monolayer, one monolayer equals the number of Rh atoms in the Rh(100) plane], a $c(2\times2)$ at $1/4<\theta<1/2$ ML, as well as a $p(2\times2)$ with pg symmetry at a coverage of exactly $\theta=1/2$ ML. In addition, very early studies indicated the formation of a $p(3\times1)$ superstructure at a coverage of $\theta=2/3$ ML and a $c(8\times2)$.[17,18] The $p(3\times1)$ structure is probably identical to the $p(3\times1)$ phase observed on PtRh alloys.[19,20]

In the present paper we report on the $c(8\times2)$ oxygen induced structure on the Rh(100) surface and analyze the geometrical structure in detail. The structure has an oxygen coverage of $\theta=1.75$ ML. Our study, a combination of low energy electron diffraction (LEED), scanning tunneling microscopy (STM), high resolution core level spectroscopy (HRCLS), surface x-ray diffraction measurments (SXRD), and density functional theory (DFT) calculations, demonstrates the formation of a surface oxide and determines the detailed geometrical structure of this oxide. The structure is shown to be a slightly distorted hexagonal trilayer of RhO_2, similar to that observed on Rh(111).[1]

II. EXPERIMENTAL AND COMPUTATIONAL METHODS

The crystals were cleaned by cycles of Ar^+ sputtering and annealing at 1200 K, followed by an oxygen treatment at temperatures up to 1100 K in order to remove residual C and a short anneal in vacuum up to 1300 K in order to remove any remaining O. The cycles were continued until no contaminants could be detected by either HRCLS or Auger electron spectroscopy (AES) and LEED displayed a sharp (1×1) pattern with low background.

The HRCLS measurements and qualitative LEED were performed at beam line I311 at MAX II in Lund, Sweden[21] using normal emission of the photoelectrons. The measurements were done at liquid nitrogen temperatures in order to reduce thermal broadening. The STM measurements were done in Vienna at room temperature using the same instrument as in Refs. 1 and 9, operated in negative sample bias. The quantitative LEED analysis was done in Vienna as well,

using the same experimental setup as described in Ref. 22. The LEED measurements were performed at normal incidence of the primary electron beam using a two-grid system and video data acquisition. The LEED patterns were stored as 8-bit images and subsequently analyzed by an image processing program which extracted the *I-V* spectra for each visible beam. After background subtraction and normalization to the emitted electron current, the *I-V* spectra were averaged over symmetry-equivalent beams and smoothed in the Fourier domain.

The LEED calculations were done using the TensErLEED program package,[23] where the tensor LEED perturbation method[24,25] is implemented. To determine the agreement between measured and calculated *I-V* curves the Pendry R-factor[26] was chosen. The error bars given in this paper were derived from Pendry's variance; to reduce the computational effort, all other parameters were fixed to the best-fit structure, hence no subsequent reoptimization was performed and the error bars do not account for coupling between search parameters. Although neglecting parameter correlations (a usual procedure) can result in an underestimation of the error limits,[27,28] the good agreement with the DFT (cf. Table I) and SXRD data indicates that the error bars obtained are still rather conservative.

The SXRD measurements were performed at the MPI-MF beamline at the Angstrom Quelle Karlsruhe (ANKA) in Germany.[29] A photon energy of 10.5 keV was used and the experiments were conducted in a six-circle diffraction mode with the sample normal in the vertical direction. The incidence angle was fixed close to the critical angle for total external reflection of Rh. The crystal basis used to describe the (H K L) diffraction is a tetragonal basis set $(\mathbf{a}_1, \mathbf{a}_2, \mathbf{a}_3)$, with $\mathbf{a}_1$ and $\mathbf{a}_2$ lying in the surface plane and of length equal to the nearest-neighbor surface distance $a_0/\sqrt{2}$, and $\mathbf{a}_3$ out-of-plane with length a_0 [a_0(Rh)=3.89 Å]. Structure factors were obtained after background subtraction and integration of rocking scans with rotation of the sample around its surface normal for different *L* values. In addition standard correction factors were applied.[30]

The *ab initio* calculations were performed in Vienna using the Vienna *Ab Initio* Simulation Package (VASP).[31] The interaction between the core and the valence electrons was treated by the projector augmented wave method[32] in the implementation described in Ref. 33. The valence wave functions were expanded in a plane wave basis set with a plane wave cutoff of 250 eV. The generalized gradient approximation (GGA) was applied throughout this work.[34] Brillouin zone integration was performed using grids corresponding to $(8\times8\times1)$ *k*-points in the primitive cell for all surface calculations. With this setup a Rh lattice constant of 3.84 Å was found in excellent agreement with experiment and previous calculations.[35–38]

The Rh substrate was described by a four layer thick slab (only the top two substrate layers are shown). The bottom two layers were fixed, whereas the top two layers were allowed to relax. The RhO_2 trilayer was placed on top of the relaxed side of the slab (asymmetric setup).

III. RESULTS

A. Qualitative examinations

Exposing the Rh(100) surface to an oxygen atmosphere of 5×10^{-5} mbar at 700 K for 600 s results in a oxygen induced LEED pattern as shown in Fig. 1. The solid lines indicate the (1×1) pattern from the Rh(100) substrate lattice. The dashed lines indicate the formation of a close-to-hexagonal overlayer on the Rh(100) substrate. Apart from the hexagonal pattern, additional spots can be seen. These are the result of a coincidence lattice of the two different structures, yielding an overall periodicity of a $c(8\times2)$ as indicated by the dotted lines in the figure. The $c(8\times2)$ periodicity implies that the hexagonal pattern is in fact slightly distorted with in-plane lattice distances of $a_1=3.09$ Å and $a_2=3.07$ Å, where $\mathbf{a}_2$ is parallel to the $[0\bar{1}1]$ direction.

These observations are directly confirmed by the STM image displaying atomic resolution as shown in Fig. 2. Apart from the obvious hexagonal appearance of the structure, the image reveals a long range undulation in the $[0\bar{1}1]$ direction, which is due to the coincidence between the hexagonal oxide overlayer and the square Rh(100) substrate. The resulting $c(8\times2)$ unit cell of the structure is indicated in the image. By simply counting the number of bright protrusions in the $[0\bar{1}1]$ direction it can be seen that seven oxide lattice distances correspond to eight substrate distances yielding a lattice distance in the oxygen induced structure of 3.07 Å in perfect agreement with the LEED observations. Careful inspection of the STM image also reveals that the structure has a true $c(8\times2)$ periodicity, not an incommensurate lattice with a periodicity close to $c(8\times2)$.

Having established the in-plane lattice distance of the oxygen induced $c(8\times2)$ structure we turn to the composition of the structure by the use of HRCLS. The Rh $3d_{5/2}$ core level spectrum (Fig. 3) reveals three components. Apart from the bulk component we find one component shifted by −0.32 eV towards lower binding energy as well as one component shifted +0.73 eV towards higher binding energy. The component at lower binding energy may be interpreted as originating from the Rh atoms at the interface between the Rh(100) crystal and the hexagonal oxide structure, since such a component is frequently observed in thin oxide/metal systems.[1,9,10,39] The higher binding energy component is most naturally attributed to highly oxygen coordinated Rh atoms, in agreement with our previous study on the surface oxide formation on Rh(111).[1]

Turning to the O 1*s* spectrum in Fig. 3, two components separated by 1.1 eV having approximately similar intensities can be seen. This directly demonstrates the presence of at least two different kinds of oxygen atoms in the $c(8\times2)$ structure. Further information on the origin of the two components may be obtained by varying the incoming photon energy and thus probing the depth in the oxide layer from which the photoemitted electrons originate. By this procedure we find that the higher binding energy component originates from oxygen atoms closer to the bulk than those causing the lower binding energy component. This is indicated as interface and surface in Fig. 3.

TABLE I. Comparison between *ab initio* (DFT) and LEED results for the structural parameters of the $c(8\times2)$ surface oxide structure on Rh(100). DFT coordinates are scaled to the experimental lattice constant of $a_0=\sqrt{2}a_s=3.80$ Å; Δx and Δy refer to the unrelaxed $c(8\times2)$ lattice, with equidistant atom spacing in the x direction (a_s for the substrate, $\frac{8}{7}a_s$ for the oxide, cf. Fig. 6). The unrelaxed y coordinates of the atoms in layer O_{1n}, Rh_{0n}, and O_{2n} are taken as $\frac{4}{3}a_s$, $\frac{2}{3}a_s$, and 0, respectively. Δz denotes the height of an atom with respect to the center of gravity of the respective layer, and interlayer distances d_{ij} (in Å) refer to the centers of gravity of the layers. The vibrational amplitudes given are for the entire layer; for the substrate layer Rh2 and below a fixed value of 0.074 Å was used.

	DFT			LEED	
Atom	Δx (Å)	Δy (Å)	Δz (Å)	Δz (Å)	Vibration (Å)
O_{11}	0	−0.03	+0.00	−0.01±0.05	0.18±0.04
O_{12}	0.01	−0.02	0.01	0.01±0.04	
O_{13}	0.02	0.01	−0.00	0.01±0.05	
O_{14}	0.01	0.02	−0.01	−0.01±0.03	
$d_{O1\text{-}Rh0}$			0.92	0.91±0.03	
Rh_{01}	−0.00	−0.00	−0.04	−0.02±0.04	0.13±0.03
Rh_{02}	−0.01	+0.00	−0.01	−0.00±0.04	
Rh_{03}	+0.00	+0.00	0.01	0.01±0.03	
Rh_{04}	+0.00	−0.01	0.02	0.01±0.02	
$d_{Rh0\text{-}O2}$			1.01	1.03±0.02	
O_{21}	0	−0.04	0.03	0.03±0.08	0.14±0.05
O_{22}	−0.03	−0.03	0.04	0.02±0.07	
O_{23}	−0.04	+0.00	0.02	0.04±0.07	
O_{24}	−0.03	+0.04	−0.07	−0.07±0.06	
$d_{O2\text{-}Rh1}$			1.91	1.90±0.03	
Rh_{11}	0	+0.01	−0.03	−0.04±0.08	0.09±0.05
Rh_{12}	0.04	+0.01	−0.02	−0.02±0.05	
Rh_{13}	0.06	−0.00	0.01	0.02±0.05	
Rh_{14}	0.06	−0.00	0.03	−0.01±0.05	
Rh_{15}	0	−0.00	−0.02	0.05±0.08	
$d_{Rh1\text{-}Rh2}$			1.87	1.89±0.02	
$d_{Rh2\text{-}Rh3}$			1.88	1.91±0.02	
d_{bulk}			1.90	1.90 (fix)	

We may also estimate the amount of oxygen and Rh present in the $c(8\times2)$ structure. For this we first note that as each hexagonal oxide cell must contain an integer number of each kind of atom, the Rh and O coverages must be an integer multiple of 7/8=0.875 ML. As stated above, at lower oxygen exposures a $p(2\times2)$ and a $p(2\times2)pg$ structure is formed with oxygen coverages of 0.25 and 0.5 ML, respectively. By comparing the signal in the O 1*s* spectrum from the $c(8\times2)$ structure with these structures, we estimate the amount of oxygen in the surface oxide to about 1.8 ML.

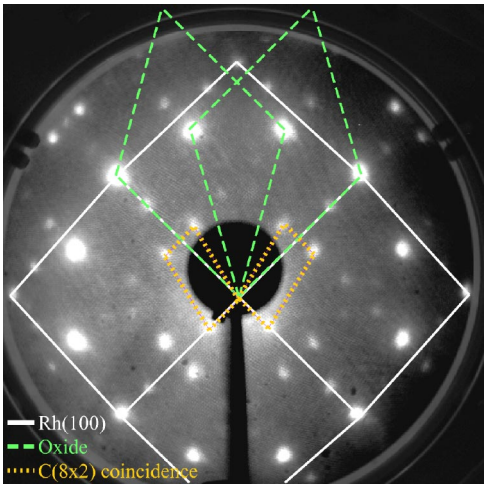

FIG. 1. (Color online) Image of the oxide induced LEED pattern at 146 eV after an oxygen exposure of 5×10^{-5} mbar for 600 s at a sample temperature of 700 K. Solid lines indicate the Rh(100) substrate pattern, dashed lines the hexagonal overlayer induced by the oxygen exposure, and dotted lines the $c(8\times2)$ pattern from the combined hexagonal oxide layer and squared substrate.

Concerning the Rh $3d_{5/2}$, the intensity of the highly oxygen coordinated Rh component is close to that of the surface component of a clean crystal. This allows us to conclude that the amount of Rh and O in the surface oxide corresponds to 0.875 and 1.75 ML, respectively, and the stoichiometry of the oxide structure is estimated to RhO_2. In summary the HRCLS measurements indicate a trilayer RhO_2 structure with two oxygen layers and one Rh layer in between, similar to the surface oxide on Rh(111).[1]

B. Structural details

The information obtained from the qualitative LEED, STM, and HRCLS measurements, as well as the insight gained from the Rh(111) surface,[1] may now be used to construct a model of the oxygen induced $c(8\times2)$ structure as shown in Fig. 4. Starting from this model, structural details, i.e., atomic coordinates, were obtained by DFT and quantitative LEED investigations and confirmed by SXRD.

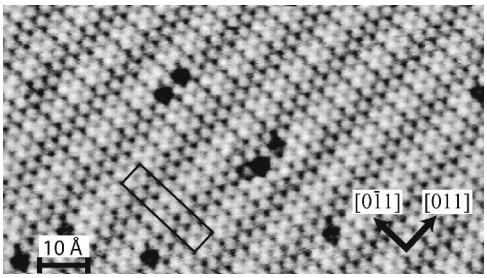

FIG. 2. STM image of the $c(8\times2)$ structure revealing a close-to-hexagonal surface structure. The longer range undulation due to the coincidence between the hexagonal oxygen induced overlayer and the square Rh(100) substrate is also revealed resulting in a $c(8\times2)$ unit cell as indicated. The tunneling parameters were −0.11 V and 1 nA.

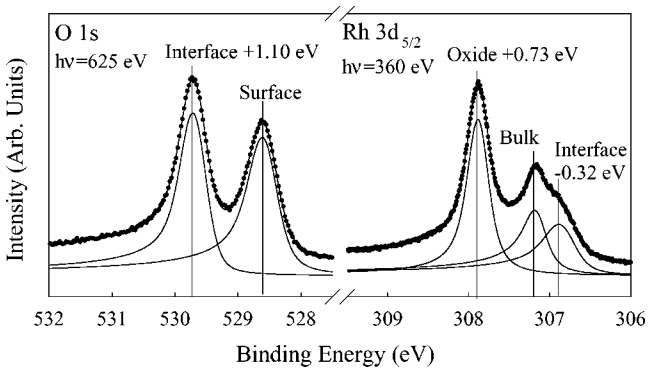

FIG. 3. HRCL spectra obtained from the $c(8\times2)$ structure. The Rh $3d_{5/2}$ level reveals three components corresponding to the bulk of the Rh crystal, the interface between the Rh crystal and the $c(8\times2)$ structure and highly oxygen coordinated Rh atoms. The O 1*s* spectrum shows two clearly discernible peaks of approximately the same intensity demonstrating the presence of two kinds of O atoms with different chemical surroundings in the $c(8\times2)$ structure.

1. DFT calculations

The final relaxed DFT model is shown in Fig. 4. The oxygen atoms in the interface layer are located in top and bridge sites of the Rh surface. An alternative model with the same trilayer oxide, but the interfacial oxygen atoms in hollow and bridge sites, is higher in energy by about 5 eV per $c(8\times2)$ cell. The preference of the atop site for interfacial oxygen atoms is common to ultrathin oxides on metals and metal-oxide interfaces and has also been observed for the trilayer structure on Rh(111),[1] as well as for ultrathin vanadium oxide layers on Pd(111) and Rh(111).[40–42]

To check the reliability of the model, we have simulated an STM image and calculated the core level shifts. The theoretical image was obtained using the Tersoff-Hamann approach,[43] simulating tunneling from filled states between −0.2 and 0 eV into the tip. The image is shown in Fig. 4(c) exhibiting overall excellent agreement with experiment [Fig. 4(d)]. The simulation indicates that the bright spots correspond to the oxygen atoms in the surface layer. The undulation in the $[0\bar{1}1]$ direction originates from the alignment of the oxygen atoms in the interface layer with the substrate. The bright stripes can be found over areas where interface oxygen atoms are located in atop position. In this position the orbitals overlap and the binding between the metal and the oxygen is large, resulting in a larger tunneling probability than in bridge sites, where binding and orbital overlaps are weak. A Rh atom bound to an atop oxygen (Rh_{01} in Fig. 6) is located in the center of the triangles of somewhat brighter O atoms marked in Fig. 4.

Additional confirmation for the correctness of the structure model is obtained from a comparison of calculated and experimental core level shifts. The core level shifts were calculated in the initial and final state approximation. In the initial state approximation one core electron is excited but no relaxation of other electrons is allowed, i.e., electronic screening of the core hole is totally neglected, whereas in the final state approximation the valence electrons are allowed to

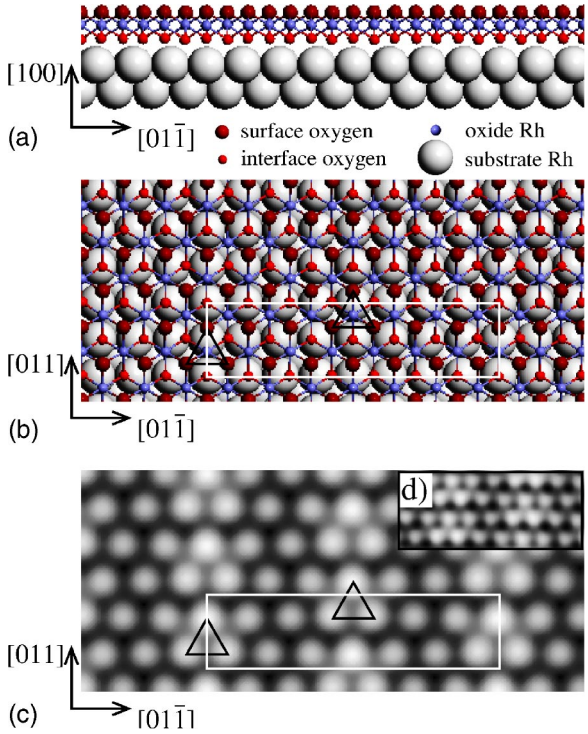

FIG. 4. (Color online) (a) and (b) The resulting model of the $c(8\times2)$) structure. (c) The simulated STM image of the $c(8\times2)$ structure. The $c(8\times2)$ cell and the bright triangels are indicated. (d) The experimental STM image after Fourier transform filtering, which averages over a few cells and thereby reduces the noise.

relax after the core electron has been removed. A more detailed discussion of the method used to calculate core level shifts in the present case can be found in Ref. 37. The calculated core level shifts are presented in Fig. 5. The agreement with the experimental results, in particular in the final state approximation, is excellent. It is remarked that DFT predicts a small broadening of about 0.2 eV for the peaks of the Rh and oxygen interface layers in the HRCLS spectra (Fig. 3) which is, however, difficult to verify in the experimental data.

The detailed geometry resulting from energy minimization is described in Table I. Small deviations from the positions in a uniformly slightly distorted hexagonal overlayer can be found and can be explained by the adsorption sites of the interface oxygen atoms. First we will focus on the vertical displacements (Δz in Table I). In the oxygen interface layer they follow directly from the adsorption sites. Oxygens in atop sites (O_{21}, see Fig. 6) relax outwards (positive *z* displacement) while oxygens in bridge sites (O_{24}) relax inwards. The *z* displacements of atoms in the Rh oxide layer follow directly from those of the oxygen atoms in the interface layer. The Rh_{01} atom is coordinated to one oxygen in atop position (O_{21}) and two oxygens in bridge sites (O_{14}). Therefore it is closer to the interface than the Rh_{04} atom, which is bound to two O atoms in (nearly) atop sites (O_{21} and O_{22}) and one O atom in a bridge site (O_{24}). In the top oxygen layer, the *z* displacements of the atoms are much smaller but can be rationalized in principle in the same way. The explanation of the in-plane displacements follows from

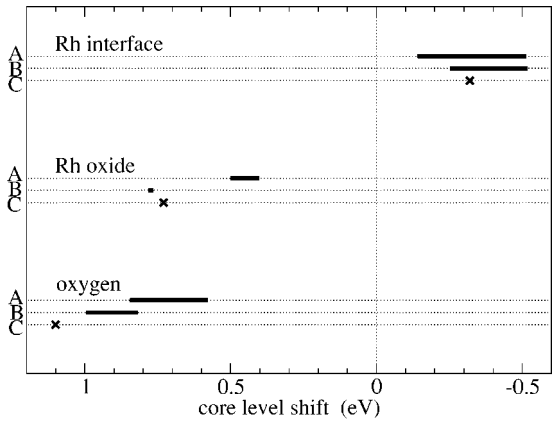

FIG. 5. Comparison between the theoretical and experimental Rh 3*d* and O 1*s* core level shifts for the $c(8\times2)$ surface oxide. For Rh the core level shifts are referred to the Rh bulk value, whereas for oxygen the O 1*s* binding energy difference between the surface and the interface O layer is shown. "A" indicates the calculated initial state shifts, "B" the calculated shifts including final state effects, and "C" shows the experimental shifts. In the calculation differently coordinated atoms in the same layer have different binding energies with the range of the calculated shifts indicated by bars.

similar arguments. Atoms with non-negligible in-plane displacements are indicated in Fig. 6 by small black arrows. The *x* displacement of the interface oxygen atoms is related to the preference to adsorb on top of Rh atoms. If the oxygen atoms are not located exactly in top sites, they and the Rh substrate atoms experience a force towards each other. Finally, we have to understand the displacement in the *y* direction which is observed for the oxygen atoms in both layers. To explain them we will pick out one oxygen atom with a relatively large shift, O_{21}, with the explanation for the other oxygen atoms being similar. The O_{21} atom is bound to the following three Rh atoms in the oxide: Rh_{01} and twice to Rh_{04}. Due to their height the O_{21} atom is closer to the Rh_{01} atom than for a uniformly compressed hexagonal overlayer, while the distance to the Rh_{04} atom is slightly increased. This yields a repulsive force away from the Rh_{01} atom and an attractive force towards the two Rh_{04} atoms. Similarly, the surface oxygen atoms are always shifted towards the lower Rh atoms in the oxide, keeping all Rh-O bonds roughly equal. The average Rh-O bond lengths in the oxide (based on DFT coordinates scaled to the experimental Rh lattice constant) are 2.00 and 2.06 Å for bonds involving surface and interface oxygen, respectively.

2. LEED analysis

For the LEED *I-V* analysis LEED patterns starting from 40 eV up to 400 eV were recorded, with an energy step of 1 eV. We could extract 16 symmetry-inequivalent beam sets (4 integer and 12 fractional order beams) with a total energy range of 3748 eV (1031 and 2717 eV, respectively).

The only structural model considered for the final LEED calculations was the oxygen induced $c(8\times2)$ structure suggested by the other experimental investigations and DFT results, shown in Figs. 4 and 6. In a first analysis (varying only

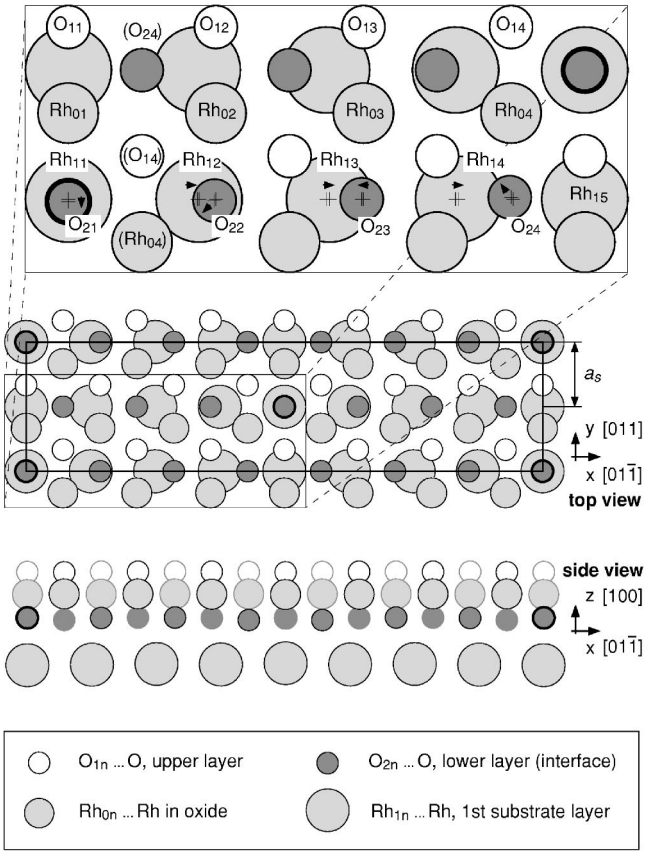

FIG. 6. Top and side view of the structural model of the oxygen induced $c(8\times2)$ structure on Rh(100) as determined by *ab initio* calculations and quantitative LEED. The oxygen atoms in on-top positions of the Rh substrate are marked by thick black circles. Atom designations in parentheses refer to equivalent positions ($c1m1$ symmetry). Small arrows in the magnified part indicate the directions of the lateral displacements of the O_{2n} and Rh_{1n} atoms.

the layer distances), other alignments of the trilayer surface oxide relative to the substrate than the on top position shown in Figs. 4 and 6 gave significantly higher Pendry R-factors (bridge and hollow positions were investigated).

For optimization, the first five interlayer distances were varied within the tensor LEED framework. In addition, buckling inside the surface oxide trilayer and the first substrate layer has been considered, as well as a variation of the vibrational amplitudes of these layers. An optimization of the in-plane coordinates was omitted since according to the DFT data rather small deviations could be expected, mostly too small for LEED's low sensitivity to these parameters at normal incidence. Furthermore, we did not want to unnecessarily increase the already rather high number of independent parameters. Thus, taking into account the $c1m1$ surface symmetry, 18 independent geometric parameters were varied in the structural search, as well as four vibrational amplitudes. The imaginary part of the inner potential was optimized fully dynamically and kept energy independent. An energy dependent real part[44] was used and its offset V_{0r} was optimized (the result given below is not corrected for the work function of the LaB_6 filament). This results in 24 independent fit parameters (18 vertical coordinates, 4 vibrational amplitudes,

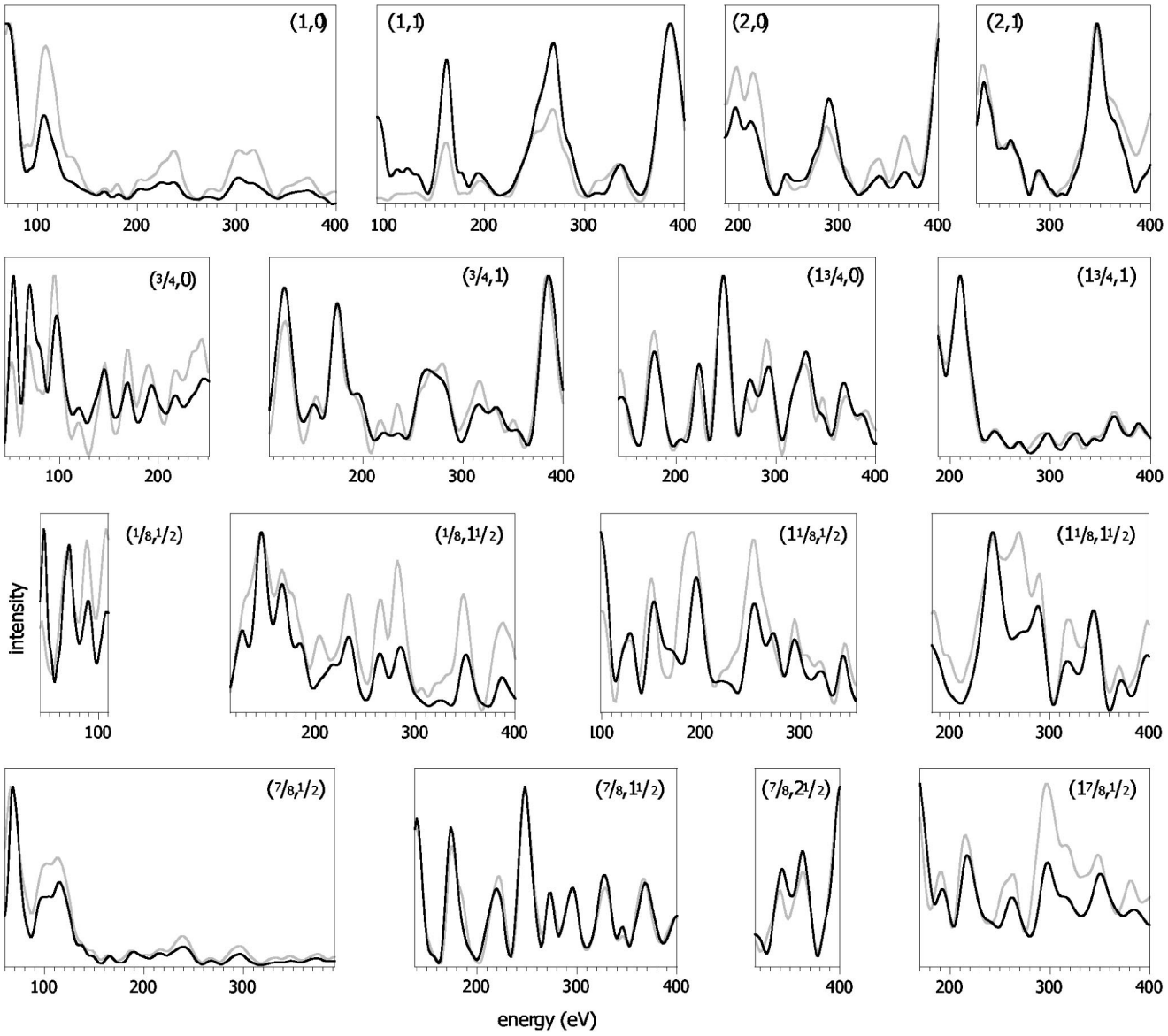

FIG. 7. Comparison between experimental (black) and calculated (gray) LEED *I-V* spectra of the best-fit model of the oxygen induced $c(8\times2)$ structure on Rh(100) ($R_{\mathrm{Pe}}=0.16$).

real and imaginary parts of the inner potential). The best-fit geometric data and the vibrational amplitudes are given in Table I, the resulting values of the inner potential are $V_{0r}=-5$ eV and $V_{0i}=5.7$ eV, and an overall Pendry R-factor of 0.16 has been achieved. A comparison of all calculated *I-V* curves, using the best-fit structure, with the measured ones is presented in Fig. 7, showing good agreement for every single beam.

Given the complexity of the structure and the large experimental database (energy range), the Pendry R-factor of 0.16 indicates that the structural model is correct. Furthermore, we find almost perfect agreement of all atomic coordinates between the DFT (calculated for $T=0$ K) and the LEED results (cf. Table I). The agreement of the interlayer distances is within about ±0.01 or ±0.02 Å, and also the small buckling amplitudes of a few hundredths of an angstrom are reproduced well. This also tells us that the room-temperature structure found by LEED is not modified by strong anharmonic vibrations, although the vibration amplitudes are almost ten times as large. We therefore regard the trilayer surface oxide model as confirmed and thus the oxygen induced $c(8\times2)$ structure as solved.

3. SXRD analysis

Since the LEED data are not sensitive enough to detect the in-plane distortions calculated by DFT, we have used SXRD for an additional confirmation of the model. Due to the large in-plane momentum transfer, SXRD has the advantage of being highly sensitive to the in-plane displacements, thus even a limited amount of SXRD data allows us to determine whether the calculated *x* and *y* coordinates are realistic. In Fig. 8 some fractional as well as integer order out-of-plane rods are shown together with simulations[45] of the structure factors by using the model as calculated by DFT (dotted line), as obtained by LEED without accounting for

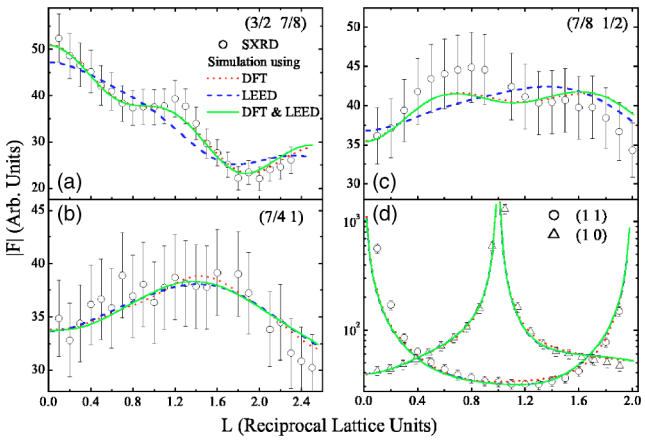

FIG. 8. (Color online) Measured structure factors from some fractional and integer order rods of the $c(8\times2)$ structure (symbols). Calculated structure factors using the model as calculated by DFT (dotted line), as obtained by LEED assuming an equidistant lattice in x and y (dashed line), and by combining the in-plane coordinates from DFT with the out-of-plane coordinates from LEED (full line).

the in-plane displacements (dashed line), and by combining the in-plane coordinates from DFT with the out-of-plane coordinates from LEED. The simulations were performed without any additional refinement of the structural parameters. Visual inspection of the measured and the calculated structure factors reveals excellent agreement, which can be taken as another strong indication that the model as obtained by LEED and DFT is correct. Using the coordinates as obtained by LEED, which used in-plane coordinates corresponding to an equidistant lattice in x and y, results in a less good agreement for the $(3/2,7/8)$ and $(7/8,1/2)$ fractional order rods. Using the DFT coordinates only or the in-plane coordinates from DFT and out-of-plane coordinates from LEED, however, both give perfect agreement. Thus the SXRD analysis can be seen as a confirmation of the in-plane coordinates calculated by DFT.

C. Phase stability

The calculated surface phase diagram is shown in Fig. 9, including the results for oxygen adsorption as well. At low coverage, oxygen adsorbs in fourfold hollow sites and forms a (2×2) structure. The situation at higher coverage was discussed intensively in the literature during the last few years. Finally, Baraldi *et al.* suggested a reconstruction, which includes the formation of threefold hollow sites where oxygen atoms prefer to adsorb.[15] In our calculations this reconstruction was indeed found to be more stable than the $c(2\times2)$ structure with oxygens in fourfold hollow sites. Concerning the surface oxide it is apparent that the O-Rh-O trilayer is thermodynamically stable, although the stability range is very narrow (50 meV).

IV. DISCUSSION

It is of course interesting to compare the present structure with that found on Rh(111).[1] It should be pointed out that the

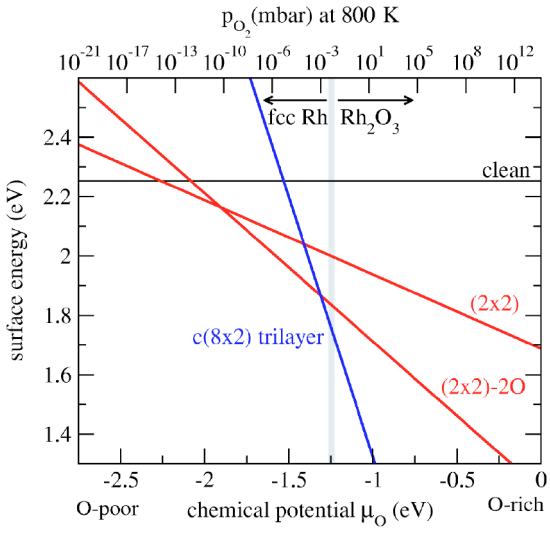

FIG. 9. (Color online) Calculated phase diagram of oxygen on Rh(100). (2×2) and (2×2)-2O refer to chemisorbed oxygen with oxygen coverages of 1/4 and 1/2 ML, respectively, with the (2×2)-2O phase denoting the structure suggested by Baraldi *et al.* (Ref. 15), where oxygen is adsorbed in threefold hollow sites. The chemical potential is related to the temperature and the oxygen partial pressure p through the ideal gas equation $\mu_O(T,p) = \mu_O(T,p^0) + 1/2k_BT\ln(p/p^0)$ (Ref. 46).

two oxides are very similar with regard to geometrical structure, and also show very similar core level spectra, despite the different crystallographic orientation of the substrate. In passing we note that this is not a general rule, e.g., the surface oxides on Pd(100) and Pd(111) do not show any clear structural similarities.

Although there are large similarities between the surface oxides on Rh(100) and Rh(111), small differences can be detected. The in-plane lattice constant of the RhO_2 trilayer on Rh(111) is found to be 3.02 Å, corresponding to (8×8) oxide units on (9×9) substrate units. This should be compared to 3.09 and 3.07 Å for the surface oxide on Rh(100) as found above. The reason for this difference is likely the substrate surface which governs the registry of the trilayer with the surface on the (100) substrate, in contrast to Rh(111) where the overlayer is essentially incommensurate and can choose its lattice parameter without any constraints from the substrate. As mentioned previously the oxygen atoms at the interface prefer to bind to substrate Rh in an on-top position and avoid the hollow sites. The commensurate $c(8\times2)$ structure avoids O in hollow sites (interface O atoms are on top of Rh or between on-top and bridge sites), but this also dictates the lattice constant of the oxide in the [011] direction (y direction in Fig. 6). Thus the in-plane interatomic distances with a nonzero y component in the oxide layer are expanded to 3.09 Å to achieve commensurability along [011]. Since the oxide will try to keep its threefold symmetry in order to maintain all Rh-O bonds in the oxide roughly equal, also the lattice distance along $[01\bar{1}]$ (i.e., in the x direction) assumes a similar value (3.07 Å), but somewhat closer to that of the unconstrained surface oxide on Rh(111). This value also allows the structure to be commensurate along $[01\bar{1}]$. The dis-

tortion of the in-plane lattice distance affects the interlayer spacing, which in turn will be restricted by the Pauli repulsion.

Another remarkable difference is that the trilayer surface oxide on Rh(100) is found to be thermodynamically stable by DFT in contrast to the situation on Rh(111) where the trilayer is only kinetically stabilized.[1] To understand the increased stability of the surface oxide on the Rh(100) substrate, we first note that the slight lattice expansion of the oxide imposed by the Rh(100) substrate is not expected to lead to a significant increase of the energy. According to our DFT calculations, the in-plane lattice constant of a free-standing RhO_2 layer is 3.1 Å, even closer to the trilayer on Rh(100) than on Rh(111), but the energy difference between lattice constants of 3.1 and 3.02 Å is so small that it is well within the error bars of DFT.

Instead, information about the increased stability can be found from the average oxygen adsorption energies, which are shown in the phase diagram as the intersection of the line of each structure with that of the clean surface. The adsorption energies found for the 1/4 ML, 1/2 ML, and trilayer structures are all about 0.2 eV higher (corresponding to lower chemical potential) on the Rh(100) substrate than on Rh(111). This is what one would expect and follows the usual trend from a more open surface to a close-packed one. For the surface oxide, the increased average oxygen adsorption energy is also related to the fact that the oxygen atoms are located exclusively in bridge and atop sites, whereas for the moiré surface oxide on the (111) substrate some interfacial oxygen atoms were located above the unfavorable hollow site. The rigid shift towards larger oxygen binding energies obviously shifts the crossing points between phases towards the left in the phase diagram indicating that Rh(100) is more easily oxidized than the Rh(111) surface. This is also experimentally confirmed, since at 700 K the surface oxide on Rh(100) forms already at oxygen pressures of 5×10^{-5} mbar, while 10^{-3} mbar is needed in order to form it on Rh(111).

A second point, however, is equally important for the increased stability of the surface oxide. The slopes of the lines for each structure is given by the oxygen coverage of each phase and are 0.25, 0.5, and $2\times7/8=1.75$, respectively, on the Rh(100) substrate. For the Rh(111) surface the corresponding slopes are 0.25, 0.5, and $2\times8^2/9^2=1.58$. For the oxide, the oxygen coverage per surface unit cell is larger on the more open surface than on the close packed (111) substrate, implying an enhanced stability of the surface oxide on the open substrate for oxidizing conditions.

V. CONCLUSIONS

We have characterized an oxygen induced structure on Rh(100) displaying a $c(8\times2)$ periodicity. Our data demonstrate that this structure is not a bulk Rh_2O_3 phase, but rather a so-called surface oxide, like recently observed thin oxide films on Pd(100),[10] Pd(111),[9] Ag(111),[8] and Rh(111).[1] The qualitative characterization was done using LEED, HRCLS, and STM measurements allowing us to understand the basics of the structure. Detailed information about the atomic coordinates of the structure were then obtained from DFT calculations and quantitative LEED measurements and confirmed by SXRD. By this procedure, we have determined the detailed atomic arrangement of this relatively complex structure.

Despite the large differences in substrate surface structure, the surface oxides found on Rh(100) and Rh(111) show essentially the same internal structure, consisting of a hexagonal trilayer of O-Rh-O. There are some differences though; for example, the structure is not perfectly hexagonal in the Rh(100) case, in contrast to the structure on Rh(111). Further the surface oxide on Rh(100) is found to be thermodynamically stable—although only in a very narrow range of chemical potentials—in contrast to the (111) case where the trilayer is only kinetically stabilized.

ACKNOWLEDGMENTS

This work was financially supported by the Swedish Research Council, the Swedish Foundation for International Cooperation in Research and Higher Education (STINT), the Austrian *Fonds zur Förderung der wissenschaftlichen Forschung*, and the EC by the NanO2, Oxidation of Nanomaterials, Specific Targeted Research Project, European Commission, Contract No. STRP 505670-1 NANO2. Support by the MAX-lab staff is gratefully acknowledged. The calculations were performed on Schrödinger II at the University of Vienna.

*Electronic address: johan.gustafson@sljus.lu.se

[1] J. Gustafson, A. Mikkelsen, M. Borg, E. Lundgren, L. Köhler, G. Kresse, M. Schmid, P. Varga, J. Yuhara, X. Torrelles, C. Quiros, and J. N. Andersen, Phys. Rev. Lett. **92**, 126102 (2004).

[2] E. Lundgren, J. Gustafson, A. Mikkelsen, J. N. Andersen, A. Stierle, H. Dosch, M. Todorova, J. Rogal, K. Reuter, and M. Scheffler, Phys. Rev. Lett. **92**, 046101 (2004).

[3] H. Over, Y. D. Kim, A. P. Seitsonen, S. Wendt, E. Lundgren, M. Schmid, P. Varga, A. Morgante, and G. Ertl, Science **287**, 1474 (2000).

[4] B. L. M. Hendriksen and J. W. M. Frenken, Phys. Rev. Lett. **89**, 046101 (2002).

[5] B. L. M. Hendriksen and J. W. M. Frenken, Surf. Sci. **552**, 229 (2004).

[6] W. X. Li, L. Sterlund, E. K. Vestergaard, R. T. Vang, J. Matthiesen, T. M. Pedersen, E. Lægsgaard, B. Hammer, and F. Besenbacher, Phys. Rev. Lett. **93**, 146104 (2004).

[7] C. Africh, F. Esch, W. X. Li, M. Corso, B. Hammer, R. Rosei, and G. Comelli, Phys. Rev. Lett. **93**, 126104 (2004).

[8] C. I. Carlisle, D. A. King, M.-L. Bocquet, J. Cerdá, and P. Sautet, Phys. Rev. Lett. **84**, 3899 (2000).

[9] E. Lundgren, G. Kresse, C. Klein, M. Borg, J. N. Andersen, M.

De Santis, Y. Gauthier, C. Konvicka, M. Schmid, and P. Varga, Phys. Rev. Lett. **88**, 246103 (2002).
[10] M. Todorova, E. Lundgren, V. Blum, A. Mikkelsen, S. Gray, J. Gustafson, M. Borg, J. Rogal, K. Reuter, J. N. Andersen, and M. Scheffler, Surf. Sci. **541**, 101 (2003).
[11] J. R. Mercer, P. Finetti, M. J. Scantlebury, U. Beierlein, V. R. Dhanak, and R. McGrath, Phys. Rev. B **55**, 10 014 (1997).
[12] A. Baraldi, V. R. Dhanak, G. Comelli, K. C. Prince, and R. Rosei, Phys. Rev. B **56**, 10 511 (1997).
[13] Y. G. Shen, A. Qayyum, D. J. O'Connor, and B. V. King, Phys. Rev. B **58**, 10 025 (1998).
[14] D. Alfe, S. de Gironcoli, and S. Baroni, Surf. Sci. **410**, 151 (1998); **437**, 18 (1999).
[15] A. Baraldi, J. Cerdá, J. A. Martín-Gago, G. Comelli, S. Lizzit, G. Paolucci, and R. Rosei, Phys. Rev. Lett. **82**, 4874 (1999).
[16] A. G. Norris, F. Schedin, G. Thornton, V. R. Dhanak, T. S. Turner, and R. McGrath, Phys. Rev. B **62**, 2113 (2000).
[17] C. W. Tucker, J. Appl. Phys. **37**, 3013 (1966).
[18] L. H. Dubois, J. Chem. Phys. **77**, 5228 (1982).
[19] P. T. Wouda, M. Schmid, W. Hebenstreit, and P. Varga, Surf. Sci. **388**, 63 (1997).
[20] M. Sporn, E. Platzgummer, E. L. D. Gruber, M. Schmid, W. Hofer, and P. Varga, Surf. Sci. **416**, 384 (1998).
[21] R. Nyholm, J. N. Andersen, U. Johansson, B. N. Jensen, and I. Lindau, Nucl. Instrum. Methods Phys. Res. A **467**, 520 (2001).
[22] E. Platzgummer, M. Sporn, R. Koller, M. Schmid, W. Hofer, and P. Varga, Surf. Sci. **453**, 214 (2000).
[23] V. Blum and K. Heinz, Comput. Phys. Commun. **134**, 392 (2001).
[24] P. J. Rous, J. B. Pendry, D. K. Saldin, K. Heinz, K. Müller, and N. Bickel, Phys. Rev. Lett. **57**, 2951 (1986).
[25] P. J. Rous, Prog. Surf. Sci. **39**, 3 (1992).
[26] J. Pendry, J. Phys. C **13**, 973 (1980).
[27] S. Müller, Ph.D. thesis, University Erlangen-Nürnberg, 1996.
[28] V. Blum, L. Hammer, W. Meier, and K. Heinz, Surf. Sci. **488**, 219 (2001).
[29] A. Stierle, A. Steinhäuser, A. Rühm, F. U. Renner, R. Weigel, N. Kasper, and H. Dosch, Rev. Sci. Instrum. **75**, 5302 (2004).
[30] E. Vlieg, J. Appl. Crystallogr. **30**, 532 (1997).
[31] G. Kresse and J. Furthmüller, Comput. Mater. Sci. **6**, 15 (1996).
[32] P. E. Blöchl, Phys. Rev. B **50**, 17 953 (1994).
[33] G. Kresse and D. Joubert, Phys. Rev. B **59**, 1758 (1998).
[34] J. P. Perdew, J. A. Chevary, S. H. Vosko, K. A. Jackson, M. R. Pederson, D. J. Singh, and C. Fiolhais, Phys. Rev. B **46**, 6671 (1992).
[35] A. Eichler and J. Hafner, J. Chem. Phys. **109**, 5585 (1998).
[36] M. Birgersson, C.-O. Almbladh, M. Borg, and J. N. Andersen, Phys. Rev. B **67**, 045402 (2003).
[37] L. Köhler and G. Kresse, Phys. Rev. B **70**, 165405 (2004).
[38] M. V. Ganduglia-Pirovano and M. Scheffler, Phys. Rev. B **59**, 15 533 (1999).
[39] C. Berg, S. Raaen, A. Borg, J. N. Andersen, E. Lundgren, and R. Nyholm, Phys. Rev. B **47**, R13 063 (1993).
[40] S. Surnev, G. Kresse, M. G. Ramsey, and F. P. Netzer, Phys. Rev. Lett. **87**, 086102 (2001).
[41] C. Klein, G. Kresse, S. Surnev, F. P. Netzer, M. Schmid, and P. Varga, Phys. Rev. B **68**, 235416 (2003).
[42] J. Schoiswohl, S. Surnev, M. Sock, S. Eck, M. G. Ramsey, F. P. Netzer, and G. Kresse, Phys. Rev. B **69**, 155403 (2004).
[43] J. Tersoff and D. R. Hamann, Phys. Rev. B **31**, 805 (1985).
[44] J. Rundgren, Phys. Rev. B **59**, 5106 (1999).
[45] The simulations were performed with the program package ROD: E. Vlieg, J. Appl. Crystallogr. **33**, 401 (2000).
[46] K. Reuter and M. Scheffler, Phys. Rev. B **65**, 035406 (2002).